Electromechanical Characterization and Computational Analysis of the Corona-Enabled Electrostatic Printed Flexible Strain Sensors

Logan G. Schmid^a, Keala M. Sunada^a, Marina G. Wong^b, and Long Wang^{c,*}

^aDepartment of Biomedical Engineering, California Polytechnic State University, 1 Grand Ave., San Luis Obispo, CA, USA 93407;

^bDepartment of Materials Engineering, California Polytechnic State University, 1 Grand Ave., San Luis Obispo, CA, USA 93407:

^cDepartment of Civil and Environmental Engineering, California Polytechnic State University, 1 Grand Ave., San Luis Obispo, CA, USA 93407

*E-mail: lwang38@calpoly.edu

ABSTRACT

Printed flexible electronics have received extensive attention due to their significant potential for advancing wearable technologies, such as for monitoring human physiological health and biomechanics. However, current manufacturing techniques (e.g., inkjet printing and screen printing) of these electronics are typically limited by high cost, lengthy fabrication times, and types of print materials. Thus, this study investigates a novel manufacturing technique, namely corona-enabled electrostatic printing (CEP), which leverages high voltage discharged in the air to attract feedstock material particles onto substrates. The CEP technique can potentially fabricate various functional materials in milliseconds, forming binder-free microstructures. This study focuses on optimizing the CEP technique to produce high-performance, flexible, piezoresistive strain sensors. Here, the strain sensors will be fabricated with carbon nanotubes (CNTs) using different discharge voltages. The effect of the discharge voltage (i.e., a critical fabrication parameter) on the sensing performance will be characterized via electromechanical testing. In addition, to better understand the sensing mechanism of the samples, finite element analysis will be performed to investigate the electromechanical response of the CEP-fabricated binder-free CNT networks. Here, computational material models will be established based on microstructures of the CNT networks, which will be acquired from experimental microscopic imaging. Overall, this study will fundamentally advance the CEP manufacturing process for flexible electronics.

Keywords: advanced manufacturing, carbon nanotubes, flexible electronics, microstructure, strain sensing

1. INTRODUCTION

Printed soft electronics (PSE) is a growing field, as these devices are playing important roles in various fields within public health as they can continuously monitor an individual's health 1,2,3. It is predicted that by 2027, the printed organic and flexible electronics market will be worth over 73 billion dollars⁴. Due to the growing applications of these devices, new manufacturing techniques have been investigated to improve the functionality of PSEs. Currently, many different PSEs have been manufactured using various two-dimensional (2D) and three-dimensional (3D) techniques such as inkjet printing, screen printing, and 3D printing⁵.

However, these techniques have limitations in efficiency and applicability when applied to soft electronics, as many of the current PSEs require a passive polymer binder for material transfer^{1,6}. Polymer binders create new limitations

such as increased drying time and low melting temperature of polymer additives, which may increase manufacturing time and costs and limit material options¹. To eliminate the need for passive polymer binders during fabrication and advance the design of PSEs, this study investigates a novel manufacturing technique, namely corona-enabled electrostatic printing (CEP)¹.

The CEP technique allows PSEs to be fabricated quickly through the material transfer in a contactless and binder-free way, which can potentially enable quick mass production of the electronics. CEP has the substrate placed in between the material and corona discharge in a non-contract way. Material transfer can occur in milliseconds, eliminating the long manufacturing time typically needed in other techniques. Further, CEP allows for more fabrication and material flexibility. Sensors fabricated with the CEP technique have been shown to allow for strain sensing, human motion monitoring, and acoustic signal detection through finite element analysis (FEA)¹.

To further investigate the strain sensing capabilities of CEP-fabricated PSEs, this study will analyze CEP- fabricated piezoresistive sensors to determine the optimal manufacturing parameters for strain sensing functionality. The performance of each sample was tested through electromechanical experiments and further characterized using FEA. In addition, to better understand the sensing mechanism of CEP-fabricated strain sensors, a customized high-precision loading device was coupled with an optical microscope to perform in-situ microscopic imaging of the sensing material networks during loading. This paper begins with an overview of the experimental details for sensor fabrication and testing. Then, the results are analyzed to determine the effect of different manufacturing parameters, particularly the fabrication voltage, on the piezoresistive performance of the CEP-fabricated sensors.

2. EXPERIMENTAL DETAILS

2.1 Materials

In this study, transparent medical tapes (Nitto, XTRATA® Perme-Roll AIRTM) were used as substrates, mainly due to their high flexibility. Carbon nanotubes (CNTs), obtained from NanoIntegris (purity $\geq 99\%$, outer diameter $\leq 13-18$ nm), were used as sensing elements.

2.2 Fabrication of Sensors

The CNT-based strain sensors were fabricated using the CEP technique, where a tungsten needle was used as an electrode to generate a corona discharge under high voltage, leading to a strong electric field in the acrylic fabrication chamber positioned below. The electric field could attract the CNTs to the substrate due to the resultant electrostatic forces. Then, conductive threads were attached to both ends of the sensor using silver paint to serve as electrodes for electrical resistance measurement. Between each sensor fabrication, the surfaces were cleaned with 70% isopropyl alcohol and an ionizing fan to remove residual charge.

Typically, during the CEP fabrication, a high discharge voltage is needed to generate the electrostatic attractions of the CNTs. In this study, to better understand the effects of the fabrication voltage on the sensing performance, multiple sensors were fabricated using eight different voltages ranging from 7.5 kV to 25 kV. The distance between the tungsten needle electrode and the substrate remained the same at 35 mm throughout all fabrications.

2.3 Strain Sensing Testing of CEP-Fabricated Sensors

The electromechanical properties of the fabricated sensors were evaluated via cyclic loading tests. A Shimadzu load machine was used to apply cyclic loading, while a Keysight digital multimeter was used to simultaneously measure and record the chsamples' resistance during loading. The load pattern consisted of 10 cycles of tensile loading at a 36% strain per minute loading rate with a maximum strain of 3%. To evaluate the repeatability of the sensing response, the samples were also subjected to a 200-cycle load pattern.

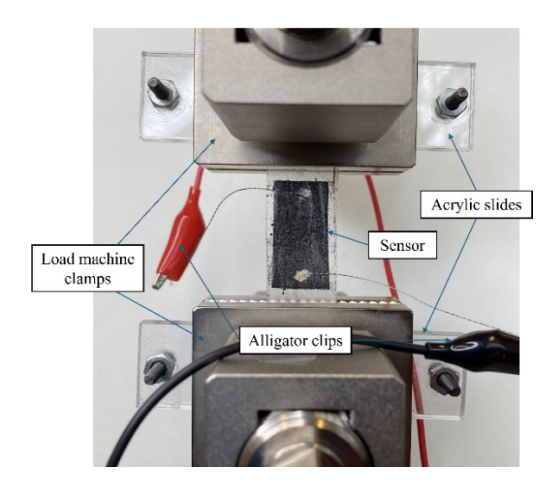


Figure 1. An optical image of the experimental setup for the electromechanical tests, where a CEP-fabricated sensor is mounted in the load machine and its resistance is measured simultaneously.

For each cyclic loading test, the sensitivity (S), or gauge factor, was calculated using Equation (1) for each cycle and averaged⁸.

$$S = \frac{R_i - R_0}{\Delta \varepsilon}$$
 (1)

Here, R_i and R_0 represent resistance measurements of the samples under loading and without loading, respectively. $\Delta \varepsilon$ denotes applied strain.

The linearity of the CEP sensor strain response was then calculated as the coefficient of determination (R²) value using a least-squares regression line (LSRL). Similarly to the sensitivity, the linearity of the loading and unloading portions of each cycle was calculated then averaged.

2.4 In-Situ Imaging of CNT Networks under Mechanical Loading

To better understand the strain sensing mechanism of the sensors, in-situ imaging of the CNT networks was conducted to monitor the microstructural change under loading. Here, a customized high-precision loading device was coupled with an optical microscope, as shown in Figure 2. Here, the samples were fabricated without a top layer of medical tape, so that the CNT particles could be directly imaged without interference from the medical tape. Each sample was mounted in the mechanical tester and placed under the microscope with the focus adjusted to ensure CNT visibility at 50x magnification. Prior to applying loads, an image was first taken for 0% strain. Then, the mechanical tester applied 4%, 8%, 12%, 16%, and 20% strains to each specimen. At each strain level, a microscopic image was taken to record the CNT network configuration.

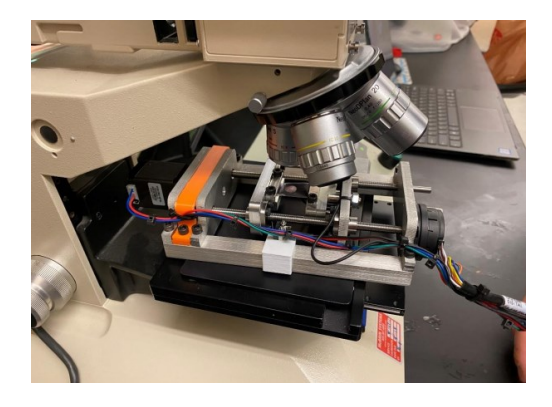


Figure 2. An optical image of the experimental setup for in-situ imaging.

In addition, to perform microstructure-based FEA of CNT networks, the microstructural images needed to be converted to computational material models. In particular, upon obtaining the images at the six aforementioned strain levels for a sample,, those images were then processed using MATLAB software. The raw images were first binarized, where small, isolated artifacts (i.e., noise) were removed. These processed images were then converted into vector-based dxf files, which could preserve the features of CNT microstructures. The dxf files were then imported into COMSOL Multiphysics software for FEA, where the Electric Current physics module was used. Here, a constant current of 2 mA was applied to the right microstructure boundary as the terminal, while the left boundary was set up as ground. The resulting terminal voltage was probed and recorded, which indicated the effective resistance of the CNT network.

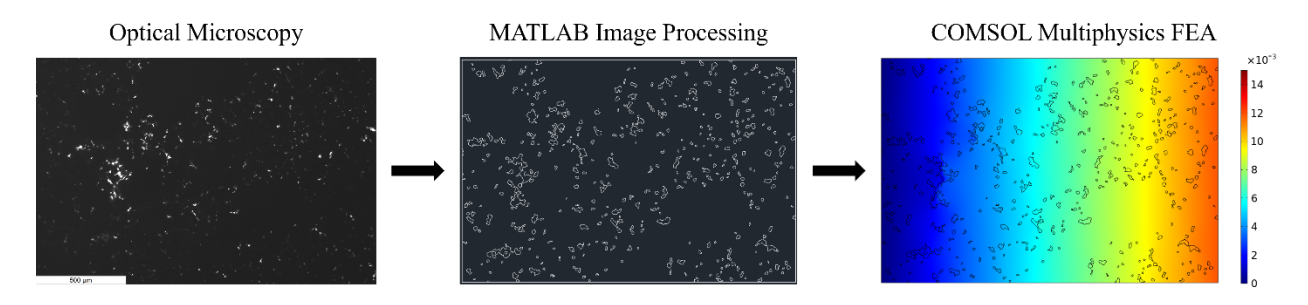


Figure 3. Workflow of microstructure-based FEA of CNT networks.

3. RESULTS AND DISCUSSION

3.1 Electromechanical Response

The samples fabricated using different voltages were subjected to cyclic tensile strains. Figure 4representative strain sensing response of the samples, which were fabricated using 25 kV, 15 kV, and 7.5 kV voltages, when subjected to 200-cycle uniaxial loading.

As shown in Figure 4a-b, the sensors fabricated at 25 kV and 15 kV displayed a very uniform response, matching up closely to the applied triangular cyclic strain pattern. Figure 4a3 and b3 show that these fabrication voltage groups exhibited R² values of 0.998 and 0.995, respectively, indicating that the CEP technique was able to produce extremely linearly performing strain sensors over a range of fabrication voltages. However, once the fabrication voltage reached a certain threshold, the sensor performance became significantly compromised. This can be seen in Figure 4c, which displays the irregular, noisy strain response of a sensor fabricated at 7.5 kV. The significantly lower R² value of 0.844 in Figure 4c3 for that cycle further suggested that 7.5 kV during CEP fabrication was an insufficient voltage to attract enough CNT particles to create a thoroughly connected CNT network, which was required to generate low-noise and reliable strain sensing response.

Figure 5 summarizes the linearity of all sensor samples tested, fabricated between 7.5-25 kV. As previously seen, the lower fabrication voltages displayed relatively lower strain response linearities. The 7.5 kV samples' average loading and unloading R² values were just under 0.70 and 0.60, respectively, which were significantly lower than other voltage groups' average linearities. The 10 kV sensors' average loading and unloading R² values were still decently strong, being 0.904 and 0.823, respectively. On the other hand, sensors fabricated at 12.5 kV and above, consistently exhibited very strong linearities with loading and unloading R² values all above 0.95. Overall, Figure 5 shows a weak correlation between fabrication voltage and the linearity of the sensing response.

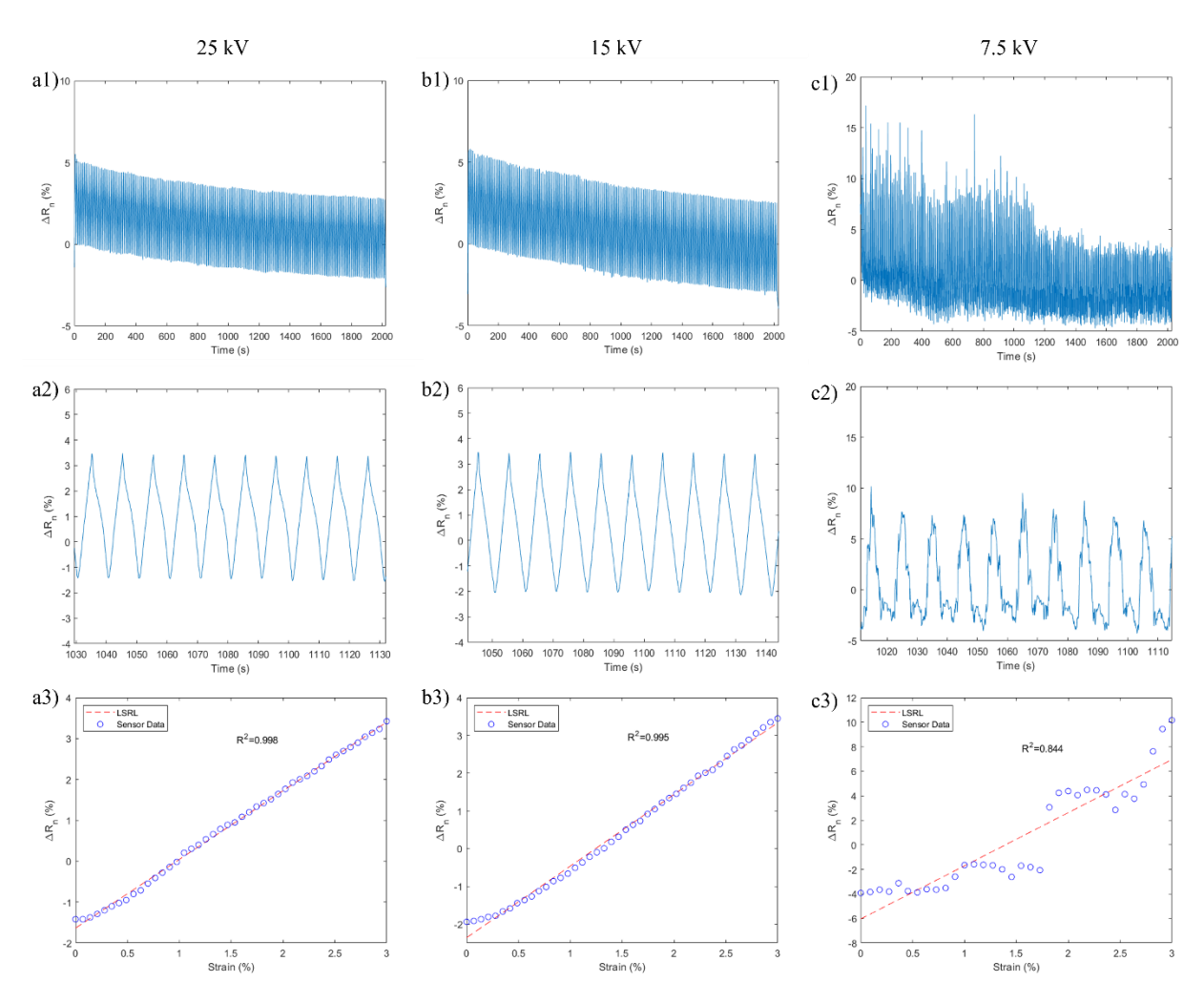


Figure 4. Strain response of CEP sensors under 200-cycle uniaxial loading. (a1-c1) Time histories of normalized resistance for the full 200 cycle loading process. (a2-c2) A zoomed-in view of 100th -110th of the 200 cycle data corresponding to (a1-c1), respectively. (a3-c3) Sensor response during the 100th loading cycle overlapped with the LSRL fit.

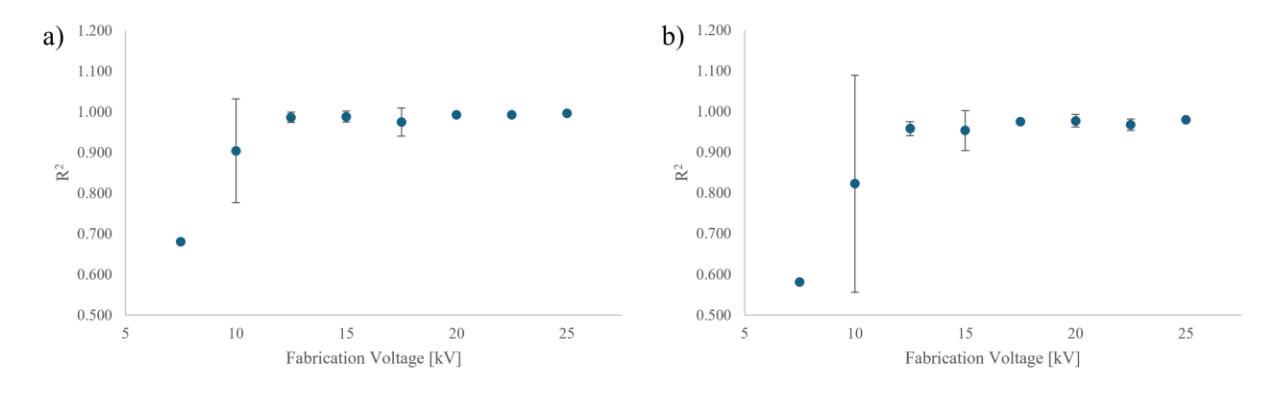


Figure 5. Summary of linearity results from (a) loading and (b) unloading portions of sensor strain responses.

In addition to linearity, strain sensitivity was the other primary quantitative performance metric of interest. The sensitivity of each sample were averaged within each fabrication voltage group and plotted in Figure 6. The average sensitivities generally valued between 1.5 - 3.0, with 12.5 kV samples averaging the lowest at 1.22 and the 7.5 kV sample being the highest at 2.85.

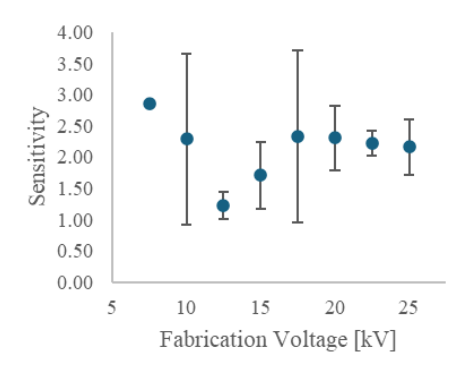


Figure 6. Summary of sensitivity results from cyclical loading

Theoretically, sensors fabricated at a lower voltage were expected to possess higher strain sensitivity. This is because a lower fabrication voltage will assemble a loose CNT network, whose connection can be more easily disturbed under mechanical loading and generate a larger change in the measured resistance. However, Figure 6 shows that there was no obvious correlation between fabrication voltage and sensitivity experimentally.

3.2 Microstructure-Based FEA

In addition to the electromechanical testing, microstructure-based FEA was performed to characterize the linearity and sensitivity of the CEP sensors. Figure 7 shows representative results of samples fabricated at 20 kV and 10 kV.

As can be seen in Figure 7a1-f1, increased strain on the CEP sensor results in a more porous CNT network with more gaps between CNTs (i.e., more white space in the microscopic image). Figure 7a2-f2 show FEA simulations yielded increased terminal voltages under larger strains. Since the injected electrical current was kept constant, the increase in normalized terminal voltage indicated an increase in normalized resistance, which demonstrated that the piezoresistive mechanism of the CEP sensors mainly stemmed from microstructural reconfiguration of the CNT networks.

It is also apparent that the 10 kV sample had a more porous CNT microstructure than the 20 kV sample, attributed to the lower electric field and CNT attraction at lower fabrication voltages. Comparing Figure 7a2-c2 and d2-f2 also supports the hypothesis that a more porous (i.e., less connected) CNT microstructure would lead to a higher sensor resistance, as the voltage plots show the 10 kV sample terminal voltages were all greater than the 20 kV sample terminal voltages at corresponding levels of strain.

In addition, the linearity of the simulated strain sensing response was also examined. Figure 7g-h show both 20 kV and 10 kV samples possessed a strong linear correlation between strain and normalized change in terminal voltage, with R² values of 0.958 and 0.919, respectively. Due to the constant applied current, this corresponded to identically strong linear correlations between strain and normalized change in resistance.

On the other hand, the greater magnitude change in normalized terminal voltage of the 10 kV sensor compared to that of the 20 kV sensor in Figure 7h and g, respectively, showcase that the lower fabrication voltage yielded a higher sensitivity. Furthermore, from the FEA results for samples fabricated at all the studied voltages, the normalized change in resistance was calculated and used to subsequently find each sample's sensitivity, as summarized in Figure 8.

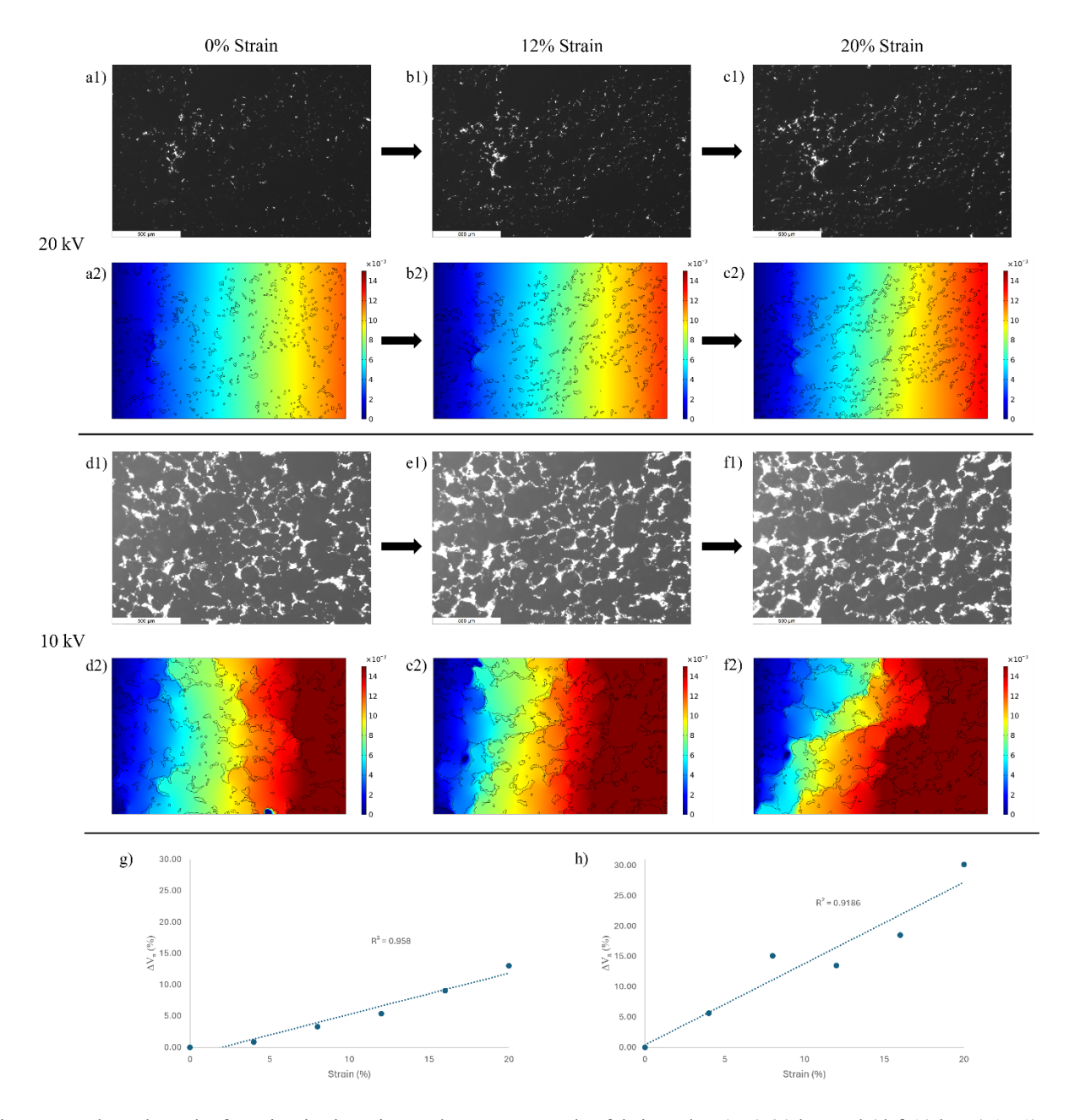


Figure 7. Selected results from in-situ imaging and FEA on samples fabricated at (a-c) 20 kV and (d-f)10 kV. (a1-c1) and (d1-f1) show the sensor imaged at 0%, 12%, and 20% strains, while (a2-c2) and (d2-f2) are the corresponding FEA results for a 20 kV and 10 kV sample, respectively. (g) and (h) depict the normalized change in terminal voltage against strain for the 20 kV and 10 kV samples, respectively.

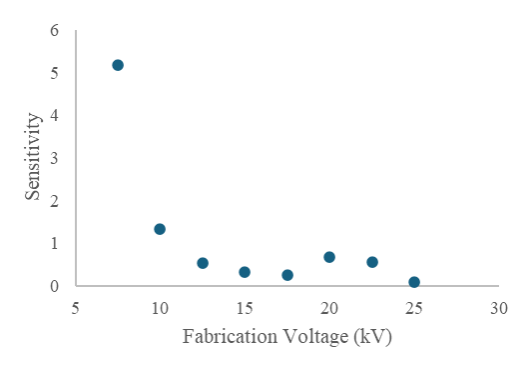


Figure 8. FEA simulated strain sensitivities of sensors fabricated at different voltages.

Similar to the cyclic loading test results in Figure 6, the sensitivities derived from the microstructure-based FEA results show little correlation between fabrication voltage and sensitivity. In this case, though, the sensor fabricated at 7.5 kV had a significantly higher sensitivity than any other samples, consistent with the previous theoretical hypothesis that lower fabrication voltages would result in a higher sensitivity due to the greater porosity of the sensor's CNT network. However, it remains desirable to have high magnitudes of both linearity and sensitivity, and as seen in Figure 5, the linearities of lower fabrication voltages like 7.5 kV are unacceptably low for real-world strain sensing applications. As a result, maintaining a balance between these two quantitative performance metrics by strategically choosing a fabrication voltage is crucial in effectively utilizing the CEP technique to produce well-performing strain sensors.

In addition, as in Figure 7g-h, the linearities of all samples tested was calculated from the microstructure-based FEA results and were summarized in Figure 9.

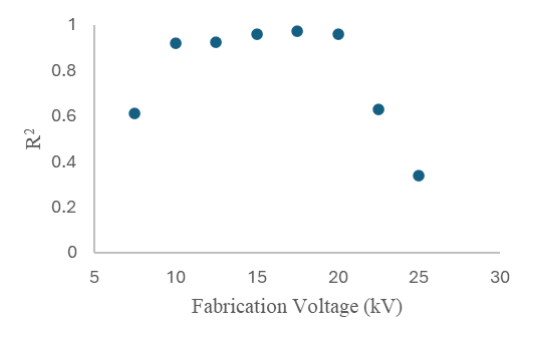


Figure 9. FEA simulation linearity results with respect to fabrication voltage

Once again, the lack of a correlation between fabrication voltage and the linearity of the sensor response is evident in Figure 9. However, unlike the strain sensing experimental measurements, among these FEA simulated results, the 25 kV and 22.5 kV samples responded with a significantly low linearity—R² values of 0.339 and 0.628, respectively. This inconsistency may be indicative of a difference in the micro-scale behavior and macro-scale response at higher fabrication voltages, where the CNT network is significantly denser than at lower voltages. At higher voltages, the CNTs may be significantly more compact to the extent that the strain-induced change in the network was not clearly visible at the optical magnification utilized in this study.

3.3 Limitations and Future Directions

Figure 4a1-c1 show the presence of low frequency decay in the CEP sensor responses' normalized resistance signal while subject to cyclical loading. The cause of this decay is outside of the scope of this study and requires further investigation. Regardless, this decay can be easily processed out to yield a sensor response with a constant baseline.

Another limitation of note is the generally low sensitivities exhibited by the tested samples compared to other similar strain sensors^{1,7}. Further work will focus on improving the sensitivity of sensors fabricated with the CEP technique up to desired magnitudes. In addition, as microstructure-based FEA requires time-consuming imaging procedures, to enrich the dataset more efficiently, one potential approach is to implement computational image reconstruction techniques to artificially generate microstructural images that can then be converted to computational material models.

Lastly, as previously mentioned, another primary limitation of this study was the low sample size in the several experimental groups due to the time-consuming nature of data collection. This made the linearity and sensitivity results collected in this study more vulnerable to variability due to human factors during fabrication and testing. More work on a greater number of samples is necessary to confirm this study's findings. One promising potential solution to this issue of low sample size in the FEA microstructure analysis is statistical image reconstruction. The stochastic image reconstruction technique enables the generation of a large database to rigorously characterize CEP-fabricated material networks at micro-scale in a low-cost and efficient manner⁸.

4. CONCLUSION

This study aims to investigate the effects of manufacturing parameters of the corona-enabled electrostatic printing technique via characterizing the sensing performance of flexible, piezoresistive strain sensors fabricated using different discharge voltages ranging from 7.5 – 25 kV. The samples were evaluated through cyclic loading tests to determine the electromechanical properties of the sensors under strain. Subsequent analysis on this data confirmed that any fabrication voltage above and including 10 kV can produce well-performing strain sensors with a high degree of linearity. Additional optical imaging in combination with in-situ mechanical loading and microstructure-based FEA indicated a similar optimal range for fabrication voltage. Overall, this study demonstrated a range of acceptable parameters for optimal performance using the corona-enabled electrostatic printing process, which has significant potential for fabricating high-performance flexible electronics.

5. ACKNOWLEDGEMENTS

This research is supported by the U.S. National Science Foundation under grant no. 2114223.

REFERENCES

- [1] Wang, L., Kou, R., Shang, Z., Weng, Z., Zhu, C., Zhong, Y. "Corona-Enabled Electrostatic Printing for Ultra-fast Manufactuing of Binder-Fee Multifunctional E-Skins," ACS Applied Materials and Interfaces 13:38, 45966-45976 (2021).
- [2] Liu, Y., Pharr, M., Salvatore, G., "Lab-on-Skin: A Review of Flexible and Stretchable Electronics for Wearable Health Monitoring," ACS Nano 11:10, 9614-9635 (2017).
- [3] Gao, W., Ota, H., Kiriya, D., Takei, K., Javey, A. "Flexible Electronics towards Wearable Sensing," Accounts of Chemical Research 52:3, 523-533 (2019).
- [4] Cruz, S., Rocha, L., Viana, J. "Printing Technologies on Flexible Substrates for Printed Electronics," Flexible Electronics (2017).
- [5] Tan, J., Farraj, Y., Kamyshny, A., Magdassi, S. "Fabrication Approaches of Soft Electronics," ACS Applied Electronic Materials 5:3, 1376-1393 (2023).

- [6] Migliorini, L., Villa, S., Santaniello, T., Milani, P. "Nanomaterials and printing techniques for 2D and 3D soft electronics," Nano Futures 6:3 (2022).
- [7] Lin, Yun-An, et al. "Graphene k-tape meshes for densely distributed human motion monitoring." Advanced Materials Technologies, vol. 6, no. 1, 6 Dec. (2020).
- [8] Kessenich, N. K., & Wang, L.. Statistical reconstruction of heterogeneous microstructures based on 2D images. Behavior and Mechanics of Multifunctional Materials XVII. (2023)